WHEC 2014
20th World Hydrogen Energy Conference 2014
June 15[Sun] – 20[Fri], 2014 KDJ Convention Center, Gwangju Metropolitan City, Korea

Combined Modelling and Experimental Analysis of a Solid Oxide Fuel Cell Stack

R.T. Nishida[a,b], S.B. Beale[a,b,c,*], J.G. Pharoah[a,b], L.G.J. de Haart[c], L. Blum[c]

[a] Dept. of Mechanical and Materials Engineering, Queen's University, Kingston, ON K7L3N6, Canada

[b] Queen's-RMC Fuel Cell Research Centre, Kingston, ON K7L3N6, Canada

[c] Forschungszentrum Jülich GmbH, Institute of Energy and Climate Research, 52425 Jülich, Germany

ABSTRACT

The proper distribution of reactant species and removal of excess heat and reaction products are fundamental to the success of solid oxide fuel cell (SOFC) stack technology. Experimental advances are limited due to the time and expense of varying the parameters over a range of designs and operating conditions. Modelling of SOFCs at the stack scale, as opposed to at the cell scale, has generally been confined to studies of the fluid distribution, neglecting any coupled effects associated with electrochemistry and/or species transport. The present work considers results from an original computational fluid dynamics (CFD) model and compares them with experimentally gathered data obtained for the Jülich Mark F stack design. The model couples the equations of momentum, heat and species transport with electrochemical reactions for large SOFC stacks with internal and external manifolds, with calculations being performed in reasonably short computation times. To validate the model, comparisons with voltage and temperature data from an 18-cell stack operating in a test furnace are made. Good agreement is obtained between the model and experiment results, confirming the validity of the methodology for stack design.

Keywords: Solid oxide fuel cell, Stack modelling, Experimental validation, Temperature distribution, Transport and electrochemistry

1. Introduction

The performance of solid oxide fuel cell stacks has improved substantially in recent years due to developments in materials and stack design through experimental analysis and modeling. For stationary applications, the design of large, powerful and durable stacks is desirable. However, in large stacks, operating concerns such as the uniform distribution of reactant species between cells and the efficient removal of excess heat and reaction products become more apparent.

* Corresponding author. Tel.:+49 2461 61-8856, E-mail address: s.beale@fz-juelich.de

Experimental advances are limited, particularly at the stack scale, by the time and expense of investigating a range of designs and operating conditions and monitoring localized effects. Therefore it is necessary to employ models with proper experimental validation to address the unique design considerations at that scale and contribute to the development of fuel cells [1-3].

Models of solid oxide fuel cells often have little or no experimental validation, or make assumptions which serve to misrepresent the characteristics of real operation. At the cell scale, a few CFD models with heat transfer and electrochemistry are compared with experimental results for simple test configurations [1,

4-8], with a range of validity, sometimes adding curve-fitting parameters.

Hydrodynamic models, with no heat transfer or electrochemistry, are commonly used to study the flow distribution in fuel cell stacks with a variety of methods [9-16], some with experimental validation [17-23] often using particle image velocimetry. However, purely hydrodynamic models neglect the effects of the reaction on species and temperature distributions, and therefore transport and other properties due to composition and temperature changes. Results from hydrodynamic models can significantly misrepresent flow distributions in realistic operating conditions and it could be misleading to attempt to design or optimize manifold configurations based on such models [24]. A few researchers have developed models capable of investigating the effects of flow paths on temperature and reaction distributions at the stack scale [25-29], each with key assumptions, and none with direct experimental validation. Peksen et al. studied the thermomechanical response of operating SOFC stacks [30,31] as well as investigated the effects of furnace vs. insulating conditions [32]. While the work focuses mainly on thermal stress analysis, it shows promise for advanced SOFC stack models with complex multiphysics.

In this work, the results of calculations for the voltage and temperature distributions for a three-dimensional computational fluid dynamics model are compared with results from an experimental programme with data for a real-life 18-cell stack. In the model solutions to the equations of conservation of mass, momentum, energy, and species transport coupled with electrochemical reactions, are obtained for the Jülich Mark F geometry, corresponding to the experimental setup in a test furnace. This work is among the first to consider a comparison with physical experiments with electrochemistry for a solid oxide fuel cell stack. Following a detailed description of the model and experimental set-up, a comparison of voltage and temperature results are presented and discussed.

2. Model Description

Flow geometry and thermo-fluid interactions impact the electrochemical performance of solid oxide fuel cells. In this work, the governing equations of mass, momentum, species and heat transport are coupled with electrochemistry and solved using the open-source CFD platform, OpenFOAM. To address limitations in computer memory and speed, a novel methodology is employed in which the diffusion terms in the reaction regions of the stack are replaced with inter-phase transfer (rate) terms. Nishida et al. [33] compare the present method with results from a previously verified model. They show that all parameters match quantitatively to within a 3% difference and require less than 1.5% the computation time.

2.1 Governing Equations

Four distinct computational domains are used to represent each of the four individual air, fuel, interconnect, and positive electrode–electrolyte–negative electrode (PEN) phases, which are to be considered as volume-averaged values. In the fluid domains, the mass (1), momentum (2), species (3), and heat (4) transport equations are applied as follows

$$\nabla \cdot (\varepsilon \rho \vec{u}) = \varepsilon \dot{m}''' \tag{1}$$

$$\nabla \cdot (\varepsilon \rho \vec{u}\vec{u}) = -\varepsilon \nabla p - \varepsilon F \vec{u} + \nabla \cdot (\varepsilon \mu \nabla \vec{u}) \tag{2}$$

$$\nabla \cdot (\varepsilon \rho \vec{u} y_i) = \nabla \cdot (\varepsilon \Gamma \nabla y_i) + \varepsilon \dot{m}_i''' \tag{3}$$

$$\nabla \cdot (\varepsilon \rho c \vec{u} T) = \varepsilon \sum \alpha_n (T_n - T) + \nabla \cdot (\varepsilon k \nabla T) + \varepsilon \dot{q}''' \tag{4}$$

where volume fractions, ε, of the individual solid/fluid phases ensure that overall species mass, force (momentum) and energy balances are correct. In the solid domains, only the energy equation, Eqn. (4), is solved. Source terms are found in each of the governing equations which are calculated as follows

$$\dot{m}_i''' = \pm \frac{i'' M_i}{v \mathcal{F} H_e} \tag{5}$$

$$q''' = \pm \frac{i''}{H_e}\left(\frac{\Delta H_T}{2\mathcal{F}} + V_{cell}\right) \quad (6)$$

$$F = \frac{2}{D_h^2} f \mathrm{Re}_h \mu \quad (7)$$

$$E = E_T + \frac{RT}{2\mathcal{F}} ln\left(\frac{x_{H_2} x_{O_2}^{0.5}}{x_{H_2O}}\right) \quad (8)$$

The current density, i'', is used in Faraday's law, Eqn. (5), to obtain the individual species and overall mass sources, $\dot{m}'''$, and the reaction enthalpy is used to prescribe a heat source, $\dot{q}'''$ in Eqn. (6). In each case, the area-based source is converted to a volumetric source by dividing by the height of the electrolyte, H_e. The distributed resistance, F, is derived from solutions for the friction factor for fully-developed flow in a channel of known aspect ratio on the cathode side, and from experimental data for pressure drop over the nickel mesh on the anode side, Eqn. (7). The inter-phase heat transfer coefficient, α_n, is calculated by harmonic averaging a shape-modified conduction term with a convective heat transfer coefficient based on known Nusselt number correlations, as is typical in heat exchanger design theory, in order to describe heat transfer between neighbouring gas-solid (and solid-solid) regions, such as air and interconnect. A mass transfer driving force, based on Sherwood number solutions is used to calculate the presence of reactant species at the electrode/electrolyte interfaces for use in the Nernst equation, Eqn. (8). An experimentally determined area specific resistance (ASR) provides overpotential effects in the relation between voltage and current density. Further information on governing equations and transport properties can be found in Nishida et al. [33].

2.2 Boundary Conditions

Uniform inlet velocities were prescribed with fixed species fractions for the air and fuel corresponding to the test conditions. A constant atmospheric pressure was prescribed at the outlet. The experimental research programme involved the conduction of tests in a furnace, which effects substantial radiative exchange with the outer sides of the stack. To account for this, a suitably linearized fourth-order radiative boundary condition is applied at the external boundaries of the model in the energy equation, with a presumed-grey emission coefficient. All other external boundaries are considered zero flux (Von Neumann), including the boundaries at the top and bottom of the stack.

3. Experimental Setup

3.1 Geometry and Structural Properties

The 18-cell SOFC stack is based on the Mark F geometry as developed at the Forschungszentrum Jülich GmbH. The Mark F design is shown in Fig. 1. The cells are of the anode substrate type as developed by Forschungszentrum Jülich. The 18 20x20cm^2 cells are manufactured with an effective electrode area of 361cm^2. Anode substrate and anode functional layer are both made of a conventional Ni/YSZ cermet. The yttria stabilized zirconia (8YSZ) electrolyte layer is around 8 µm in thickness. A Gd-doped Ce-oxide layer is applied on the electrolyte prior to depositing the LSCF cathode to prevent the inter-diffusion of cathode constituents into the zirconia electrolyte layer. The interconnect plates with integrated manifold structures for a counter-flow configuration of the reactants are machined from CroFer22APU steel.

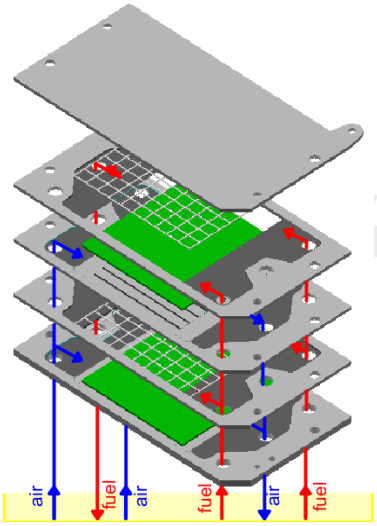

Figure 1 – Schematic illustration of the Mark F design for SOFC stacks with planar anode substrate type cells

A Ni-mesh is spot-welded to one side of the interconnect plate providing a low resistant interface with the anode substrate. The Ni-mesh simultaneously acts as fuel gas distributor over the anode area. On the other side of the interconnect plates channels are machined in the plates for distributing the air over the cathode area. On the ribs between the channels a Mn-oxide layer and a perovskite type (LCC10) oxide layer are deposited providing the low resistant interface with the cathode. For sealing a glass-ceramic sealant from the BCAS-system is used.

3.1 Test Furnace

The stack is located in the centre of a top hat furnace (see Figure 2) on an insulation stone which is about 10 cm thick. Fuel and air are supplied from the bottom in a counter flow arrangement. The gases are pre-heated electrically to the required inlet temperature. The gas temperatures are measured in the piping directly below the furnace base insulation. The loading of the stack is applied via a massive metal plate and a metal rod, which is loaded from outside the furnace with a crank system.

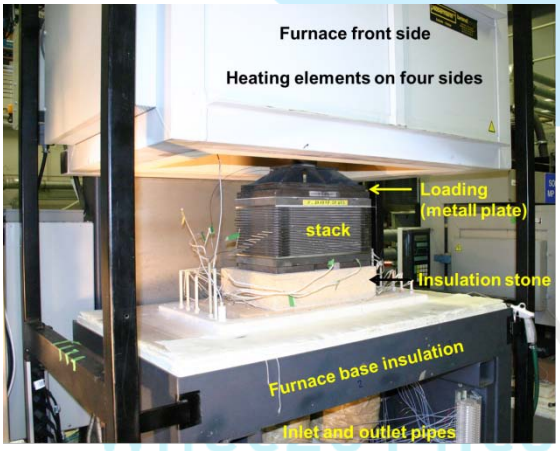

Figure 2 - Test Furnace

3.2 Measurements

The temperature of the stack was measured by thermocouples located at different positions. The thermocouple wells were located 10mm inside the interconnect and compression plates. Fig. 3 shows the positions of the thermocouples as well as the locations of the temperature plots. In order to measure the in-plane temperature profile, seven thermocouples were placed along the gas flow direction in the middle layer of the stack. The thermocouples were positioned in a way that the temperatures inside the manifold region, near the edges of the cell and near the center of the cell could be measured.

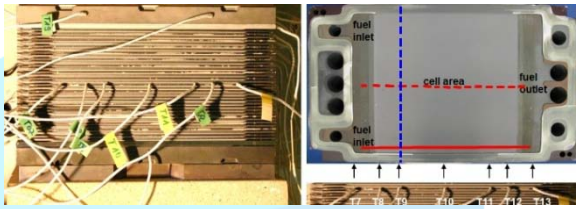

Figure 3 – Thermocouple positions. The red and blue lines represent the locations of the temperature plots in the results.

3.3 Operating Conditions

The 18-Cell SOFC stack was operated on 90 vol% H_2 and 10 vol% H_2O on the anode side and dry air on the cathode side by stepwise increasing the current every two minutes. Measurements were taken at a current density of 500mA/cm^2 or total current of 180A for an active area of 361 cm^2 cell. Inlet temperatures were measured as 675°C for both air and fuel at a location along the fuel header below the stack. The utilisation for air and fuel were 30% and 80% respectively.

4. Results and Discussion

After supplying the available input data such as geometry, inlet temperatures, furnace temperatures, mean current density, utilisations, and physical properties, calculations were performed using the CFD code from which the results of the calculations in terms of gas flow, species mass/mole fraction, temperature, current and cell voltages were output. The measurable outputs of individual cell voltage and temperature distributions are compared.

3.3 Temperature distributions

The temperature distribution in the interconnect is shown in Fig. 4. The fuel travels from left to right across the reaction region. The maximum temperature is located near the air outlet on the left, as the air has a higher flow rate and a higher heat capacity and carries heat from the reaction towards the outlet.

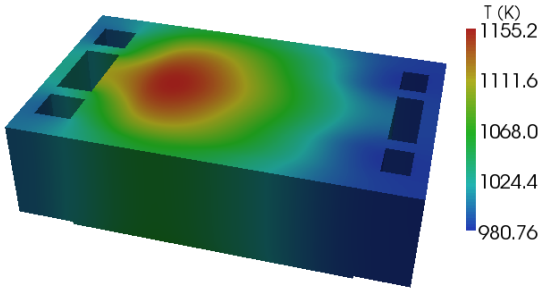

Figure 4 - Temperature distribution in interconnect

Temperatures from the model were extracted along a line 10mm deep into the interconnect at the middle cell layer corresponding to the measurement locations in the experiment. The comparison is shown in Fig. 5.

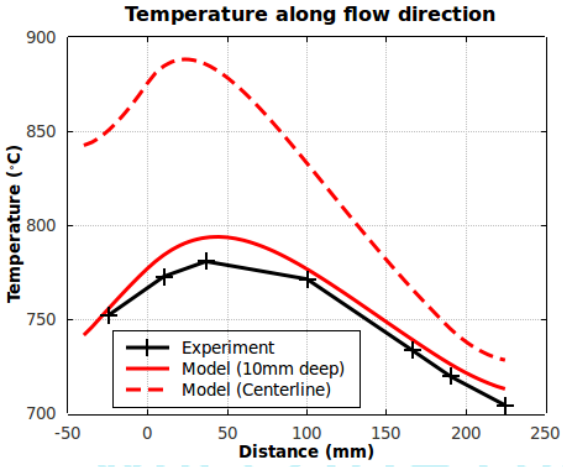

Figure 5 – Comparison of temperature distribution along flow direction in cell 9 of an 18-cell SOFC stack

The model shows a higher overall temperature distribution at the measurement location with a maximum difference of 12.6°C or 1.6%. The difference is possibly due to heat loss in the experimental set-up between the location of the measured gas inlet temperatures and the inlet used in the model. Along the centerline of the stack, away from external boundaries where heat is lost due to radiation in the furnace, the temperature reaches a higher maximum, approximately 100°C hotter.

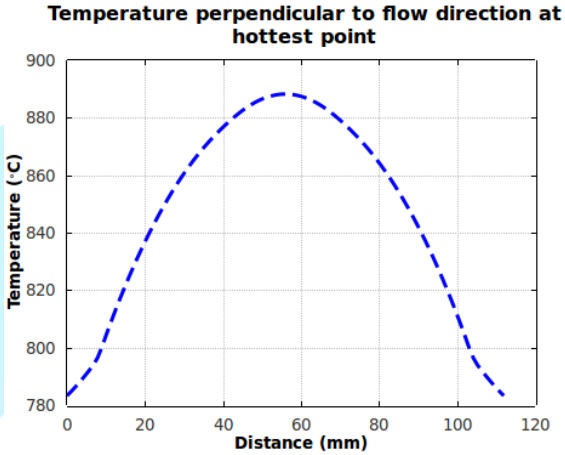

Figure 6 – Temperature distribution of model at a distance of 25mm along the flow direction.

At 25mm along the centerline, the temperature reaches 888°C as seen in Fig. 5. Temperatures at a line perpendicular to the flow direction at 25mm (see Fig. 3) are shown in Fig. 6. The temperature ranges by approximately 105°C between the two external surfaces exposed to the furnace conditions showing the influence of radiation conditions. The maximum temperature is found at the centerline.

3.3 Voltage distributions

The voltage in the stack was measured at each cell in both the model and experiment. Results are shown in Fig. 6. In the experimental set-up, metal blocks are located at the top and bottom of the stack, and the furnace heating element is located at the top of the stack. Heat is lost through the top and bottom of the stack which would help to explain the lower voltage at those cells. The heating element is located at the top of the stack which could skew the temperature distribution to be higher towards the higher cell numbers. A higher temperature would lower the area specific resistance and increase the voltage which

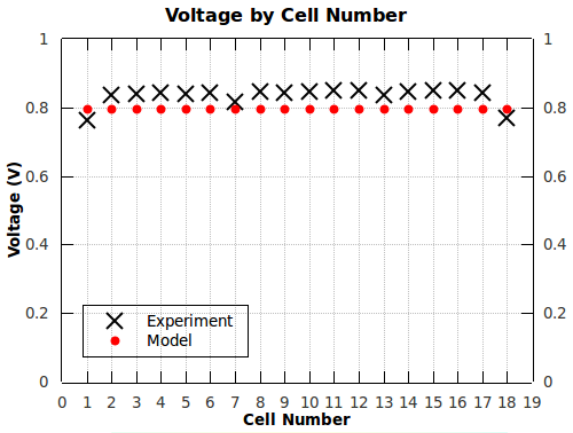

Figure 7 – Comparison of voltage by cell number for model and experiment

could help to explain the steady increase in voltage towards the top of the stack. The model has zero flux conditions at the top and bottom of the stack leading to a more constant voltage. A lower voltage of 40mV results in 10% more waste heat which could result in the increased temperature values of the model. An ASR function which more accurately reflects the experimental setup could help to increase the estimated voltage and reduce the estimate temperatures to match the experiment more closely.

5. Conclusion

Voltage and temperature distributions from a 3-D CFD model compared with those from an 18-Cell SOFC stack in a test furnace. The comparison shows good overall agreement for temperature distribution with a maximum percent difference of 1.6%. The results from the model predict a higher temperature possibly due to heat loss in the experimental set-up between the location of the measured inlet temperature and the inlet. The model assumes no heat loss in the distribution header. The model underpredicts the measured voltage possibly due to a misrepresentation of the area specific resistance. The lower predicted voltage means a higher predicted waste heat which would contribute to the increased temperature distribution seen in the model. The ASR function should be re-evaluated to more accurately reflect the experiment. This work is among the first to conduct experimental validation of a comprehensive CFD model which couples heat and mass transport with electrochemistry using a realistic SOFC stack design.

Acknowledgements

Financial support was provided by the Natural Science and Engineering Research Council through the Solid Oxide Fuel Cell Canada Strategic Research Network.

REFERENCES

[1] N. Autissier et al., “CFD simulation tool for solid oxide fuel cells”, J. of Power Sources, Vol.131, No.1, pp313–319, (2004).

[2] M.A. Khaleel et al., “A finite element analysis modeling tool for solid oxide fuel cell development: coupled electrochemistry, thermal and flow analysis in MARC®”, J. of Power Sources, Vol.130, No.1, pp. 136–148, (2004).

[3] S.B. Beale et al., “Computer methods for performance prediction in fuel cells”, J. of Power Sources, Vol.118, No.1, pp79–85, (2003).

[4] D. Larrain et al., “Generalized model of planar SOFC repeat element for design optimization”, J. of Power Sources, Vol.131, No.1, pp304–312, (2004).

[5] D. Larrain et al., “Modeling and experimental validation of solid oxide fuel cell materials and stacks”, J. of the European Ceramic Society, Vol.25, No.1, pp2627–2632 (2005).

[6] H. Yakabe et al.,“3-D model calculation for planar SOFC”, J. of Power Sources, Vol.102, No.1, pp144–154 (2001).

[7] S. Bedogni et al., “Experimental analysis and modeling for a circular-planar type IT-SOFC”, J. of Power Sources, Vol.171, No.2, pp617–625, (2007).

[8] O. Razbani et al., "Three dimensional CFD modeling and experimental validation of an electrolyte supported solid oxide fuel cell fed with methane-free biogas." Int'l J. of Hydrogen Energy, Vol.38, No.24, pp10068-1008, (2013).

[9] R.J. Boersma et al., “Distribution of gas flow in internally manifolded solid oxide fuel-cell stacks,” J. of power sources, Vol.66, No.1, pp41-45, (1997).

[10] R.J. Boersma et al., “Computational analysis of the

gas-flow distribution in solid oxide fuel cell stacks," J. of power sources, Vol.63, No.2, pp215-219, (1996).
[11] S.B. Beale et al., "Towards a virtual reality prototype for fuel cells," Phoenics J. of Computational Fluid Dynamics and its Applications, Vol.13, No.3, pp287-295, (2000).
[12] R.J. Kee et al., "A generalized model of the flow distribution in channel networks of planar fuel cells," J. of power Sources, Vol.109, No.1, pp148-159, (2002).
[13] J.H. Koh et al., "Pressure and flow distribution in internal gas manifolds of a fuel- cell stack," J. of Power Sources, Vol.115, No.1, pp54-65, (2003).
[14] W.L. Huang et al., "Flow distribution in U-type layers or stacks of planar fuel cells," J. of Power Sources, Vol.178, No.1, pp353-362, (2008).
[15] C.H. Chen et al., "Flow distribution in the manifold of PEM fuel cell stack," J. of Power Sources, Vol.173, No.1, pp249-263, (2007).
[16] W. Bi et al., "A key geometric parameter for the flow uniformity in planar solid oxide fuel cell stacks," Int'l. J. of Hydrogen Energy, Vol.34, No.9, pp3873-3884, (2009).
[17] P. Costamagna et al., "Fluid dynamic study of fuel cell devices: simulation and experimental validation," J. of Power Sources Vol.52, No.2, pp243–249, (1994).
[18] B. Chernyavsky et al., "Numerical Investigation of Flowfield in PEM Fuel Cell Stack Headers," Energy Procedia, Vol.29, pp102-111, (2012).
[19] B. Chernyavsky et al., "Turbulent flow in the distribution header of a PEM fuel cell stack," Int'l J. of Hydrogen Energy, Vol.36, No.12, pp7136-7151, (2011).
[20] J. Lebæk et al., "Particle image velocimetry and computational fluid dynamics analysis of fuel cell manifold," J. of Fuel Cell Science and Technology, Vol.7, No.3, 031001, (2010).
[21] J. Lebæk et al., "Flow and pressure distribution in fuel cell manifolds," J. of Fuel Cell Science and Technology, Vol.7, No.6, 061001, (2010).
[22] L. Grega et al., "Flow characterization of a polymer electronic membrane fuel cell manifold and individual cells using particle image velocimetry," J. of Fuel Cell Science and Technology, Vol.4, No.3, pp272-279, (2007).
[23] M. McGarry et al., "Effects of inlet mass flow distribution and magnitude on reactant distribution for PEM fuel cells," J. of Fuel Cell Science and Technology, Vol.3, No.1, pp45-50, (2006).
[24] R.T. Nishida et al., "Computational fluid dynamics modeling of heat and mass transport in solid oxide fuel cell stacks," submitted to J. of Power Sources, (2014).
[25] P. Yuan, "Effect of inlet flow maldistribution in the stacking direction on the performance of a solid oxide fuel cell stack," J. of Power Sources, Vol.185, No.1, pp381-391, (2008).
[26] S.B. Beale et al., "A distributed resistance analogy for solid oxide fuel cells," Numerical Heat Transfer, Part B, Vol.47, No.6, pp.573-591, (2005).
[27] W. Bi et al., "A key geometric parameter for the flow uniformity in planar solid oxide fuel cell stacks," Int'l. J. of Hydrogen Energy, Vol.34, No.9, pp3873-3884, (2009).
[28] M.A. Khaleel et al., "A finite element analysis modeling tool for solid oxide fuel cell development: coupled electrochemistry, thermal and flow analysis in MARC®," J. of Power Sources, Vol.130, No.1, pp136-148, (2004).
[29] K. Lai et al., "A quasi-two- dimensional electrochemistry modeling tool for planar solid oxide fuel cell stacks," J. of Power Sources, Vol.196, No.6, pp3204-3222, (2011).
[30] M. Peksen, "A coupled 3D thermofluid-thermomechanical analysis of a planar type production scale SOFC stack," Int'l. J. of Hydrogen Energy, Vol.36, pp11914-11928, (2011).
[31] M. Peksen et al., "3D transient thermomechanical behaviour of a full scale SOFC short stack," Int'l. J. of Hydrogen Energy, Vol.38, pp4099-4107, (2013).
[32] M. Peksen, "3D thermomechanical behaviour of solid oxide fuel cells operating in different environments," Int'l. J. of Hydrogen Energy, Vol.38, pp13408-13418, (2013).
[33] R.T. Nishida et al., "Comparison of solid oxide fuel cell stack performance using detailed and simplified models," Proc. Of 11th ASME Fuel Cell Conf., ES-FuelCell2013-18137, pp1-10, (2013).